Available online at www.sciencedirect.com
SCIENCE DIRECT
International Journal of Heat and Mass Transfer 49 (2006) 3831–3845
International Journal of HEAT and MASS TRANSFER
www.elsevier.com/locate/ijhmt

# A foam engulfment model for lost foam casting of aluminum

D.A. Caulk *

*Manufacturing Systems Research Laboratory, General Motors Research and Development Center, 30500 Mound Road, Warren, MI 48090-9055, United States*

Received 9 November 2005; received in revised form 14 April 2006
Available online 21 June 2006

**Abstract**

In lost foam casting of aluminum, pressure equilibrium between the liquid metal and the decomposing foam can produce a variety of different shapes for the metal flow front, ranging from convex to concave. In extreme cases, the flow front can become so strongly concave that small pieces of the foam pattern begin to break off inside the concave hollow of the flow front and become enveloped by the advancing liquid metal. When this happens, the entire mechanism of foam decomposition changes from steady ablation to a more chaotic motion in which the metal seems to "chew" its way through the pattern, creating large bubbles of vaporizing polymer liquid in its wake. These bubbles usually lead to undesirable anomalies in the final casting. In most cases, the nonlinear equations that govern the shape of the flow front depend on a single nondimensional number, which relates the onset of the engulfing motion to specific material, geometric, and process parameters. Numerical solutions to these equations are obtained for several special cases. These solutions help to explain a number of experimental observations that until now have been poorly understood.


*Keywords:* Lost foam; Casting; Engulf; Decomposition; Model

## 1. Introduction

### 1.1. Lost foam casting

Lost foam casting is a relatively new foundry process that uses an expendable pattern made of molded polymer foam. The pattern is coated with a refractory material and placed inside a steel flask, where it is surrounded with loose, dry sand. After the sand is compacted by vibration, liquid metal is poured directly into the pattern, which decomposes ahead of the advancing liquid metal as gas and liquid products from the receding foam diffuse through the porous coating and into the sand. The liquid metal eventually replaces all the volume occupied by the foam pattern before it solidifies [1].

One of the important technical challenges in lost foam casting is to understand the connection between the mechanics of foam decomposition during mold filling and the formation of internal porosity or *folds* (pairs of poorly fused metal surfaces contaminated by oxide and/or carbon residue) in the final cast product [2]. Most experts agree that such anomalies occur because some of the foam decomposition products get trapped inside the liquid metal as the mold fills.

Mold filling behavior in lost foam casting is very different from that found in other casting processes because the liquid metal has to displace more than just air to fill the mold cavity. Even though air still occupies about 97% of the cavity volume in a lost foam mold, that air is distributed among millions of tiny closed cells that form the structure of the expanded polymer foam. Before the metal can displace the air in these cells, it must first break down the thin polymer membranes that separate them. As it does, some of the foam decomposition products can mix with the liquid metal to create gas porosity or folds in the final casting. Exactly how this happens has so far eluded a conclusive explanation. Miller [3] conjectured that "turbulent" motion of the liquid metal near the flow front entrains some of the foam decomposition products before they ever

* Tel.: +1 586 986 0453; fax: +1 586 986 0574.
*E-mail address:* david.a.caulk@gm.com

0017-9310/$ - see front matter © 2006 Elsevier Ltd. All rights reserved.
doi:10.1016/j.ijheatmasstransfer.2006.04.015

**Nomenclature**

| | |
|---|---|
| $a$ | coefficient in Arrhenius expression for vaporization rate, kg/s m$^2$ |
| $A$ | temperature coefficient in expression for viscosity of liquid foam, 1/K |
| $c_A$ | specific heat of the air in the foam, J/kg K |
| $c_D$ | average specific heat of the liquid foam in the decomposition layer, J/kg K |
| $c_S$ | specific heat of the solid polymer in the foam, J/kg K |
| $d$ | pattern thickness, m |
| $D$ | nondimensional number defined by (4.21) |
| $\mathbf{e}_i$ | unit Cartesian base vectors ($i = 1, 2$) |
| $E$ | Engulf number, m$^{-1}$ |
| $E_A$ | activation energy in Arrhenius expression for vaporization rate, J/mol |
| $g$ | acceleration of gravity, m/s$^2$ |
| $G$ | nondimensional number defined by (4.21) |
| $H_0$ | metal head at $y = 0$, m |
| $H_M$ | latent heat of fusion per unit mass for the polymer in the foam, J/kg |
| $\mathbf{k}$ | vertical unit vector |
| $k_i$ | direction cosines of vertical unit vector ($i = 1, 2$) |
| $k_D$ | bulk thermal conductivity of the liquid foam in the decomposition layer, W/m K |
| $l_D$ | thickness of the decomposition layer, m |
| $L$ | length of the foam core inside hollow of concave flow front, m |
| $M_V$ | mass-average molecular weight of the polymer vapor in the decomposition layer, kg/mol |
| $n$ | exponent in Arrhenius expression for vaporization rate |
| $\mathbf{n}$ | outward unit normal vector to metal flow front |
| $p_0$ | atmospheric pressure, Pa |
| $p_D$ | pressure in the decomposition layer, Pa |
| $p_G$ | gas generation pressure, Pa |
| $p_M$ | pressure in the liquid metal, Pa |
| $p_M^0$ | pressure in the liquid metal at $y = 0$, Pa |
| $P$ | Profile number |
| $Q$ | volume flow rate of liquid foam through decomposition layer, m$^3$/s |
| $r$ | deviation of metal flow front from plane, m |
| $\mathbf{r}$ | position vector to metal flow front, m |
| $r_0$ | uniform radius of curvature of metal flow front, m |
| $r_V$ | mass rate of polymer vaporization per unit area at the metal surface, kg/s m$^2$ |
| $R$ | universal gas constant, J/mol K |
| $s$ | arc length along metal flow front, m |
| $t$ | time, s |
| $u$ | mold filling speed, m/s |
| $u_n$ | normal velocity of metal flow front, m/s |
| $v$ | velocity of the liquid foam in the decomposition layer, m/s |
| $v_A$ | average velocity of the liquid foam in the decomposition layer, m/s |
| $x$ | Cartesian coordinate, m |
| $x_V$ | mass fraction of polymer liquid vaporized in the decomposition layer |
| $y$ | Cartesian coordinate, m |

*Greek symbols*

| | |
|---|---|
| $\varepsilon_P$ | energy per unit mass required to "melt" the foam, J/kg |
| $\theta$ | temperature of the liquid foam, K |
| $\theta_0$ | initial temperature of the pattern and sand, K |
| $\theta_D$ | average temperature in the decomposition layer, K |
| $\theta_M$ | temperature on the metal surface, K |
| $\theta_P$ | nominal melting temperature of the foam pattern, K |
| $\kappa$ | curvature of the metal flow front, m$^{-1}$ |
| $\boldsymbol{\lambda}$ | unit tangent vector to metal flow front |
| $\lambda_D$ | Peclet number in the decomposition layer |
| $\mu_0$ | viscosity coefficient, Pa s |
| $\mu_D$ | effective viscosity of the liquid foam in the decomposition layer, Pa s |
| $\rho_A^0$ | density of the air in the pattern at its initial pressure and temperature, kg/m$^3$ |
| $\rho_D$ | average density of the liquid foam in the decomposition layer, kg/m$^3$ |
| $\rho_F$ | partial density of the polymer in the foam, kg/m$^3$ |
| $\rho_M$ | density of the liquid metal, kg/m$^3$ |
| $\rho_P$ | total density of the foam pattern, kg/m$^3$ |
| $\rho_S$ | density of the polymer in the foam, kg/m$^3$ |
| $\tau$ | surface tension of the liquid metal, N/m |
| $\varphi$ | volume fraction of air in the foam |
| $\psi_C$ | contact angle between the liquid metal and the coating |
| $\omega$ | non-dimensional number defined by (3.7) |

reach the coating. Zhao et al. [4] hypothesize that residual polymer liquid is not absorbed at all by the coating. Instead it lays up on the inside surface of the coating, where it vaporizes after the liquid metal passes by. These authors believe that the gas bubbles produced when this happens are responsible for the porosity and folds sometimes found in lost foam castings. Unfortunately, no one has ever modeled the mechanics of either mechanism, nor explained why some castings are almost free of such anomalies and others have them in abundance.

Recent real-time X-ray imaging by Sun et al. [5] provides a graphic picture of how some gas bubbles form

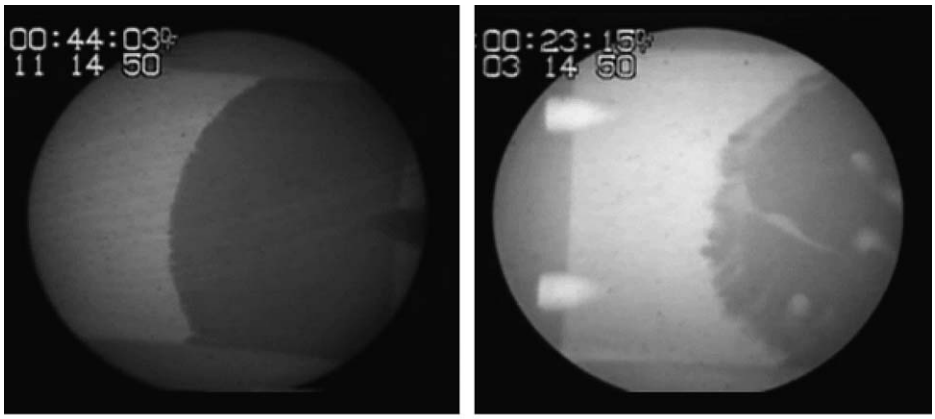


Fig. 1. X-ray images of mold filling in a rectangular plate pattern with normal coating (a) and coating with 20 times the permeability (b), from [5]. Copyright 2002 American Foundry Society, Schaumburg, Illinois, USA (www.afsinc.org). Reprinted with permission.

during mold filling. Fig. 1a shows a still image taken from a real-time X-ray video of mold filling in an 8-mm thick plate pattern, standing on edge in a sand mold. The foam decomposes ahead of the liquid metal in an even, almost symmetric pattern, emanating from a single inlet on the right side of the plate. Fig. 1b shows what happens when the coating permeability on the same pattern is increased about 20-fold. The foam decomposes almost three times faster while the metal fills the mold in about the same general sequence, but this time large bubbles form in the liquid metal just behind the flow front. Some of these bubbles stay in place and others float to the top of the casting. Not surprisingly, the second casting, unlike the first, was full of internal porosity and folds [5].

In separate experimental studies, Wang et al. [6] and Hill et al. [7] found that two entirely different patterns could be cast with almost no anomalies as long as the filling speed did not exceed a certain value. Above that speed, which was different in each casting, porosity and folds suddenly began to appear. Along with the X-ray images discussed earlier, these studies suggest that as filling speed increases, the foam decomposition mechanism suddenly changes from one that creates almost no anomalies to one that produces them in large quantities. This paper traces the origin of that change to pressure equilibrium on the metal flow front.

### 1.2. Engulfing motion

Under normal circumstances, the liquid metal decomposes the foam pattern by steady ablation [8]. This is called *contact mode*. Under the intense heat of the liquid metal, the polymer structure of the foam pattern breaks down, forming a liquid foam that occupies a narrow band between the liquid metal and the foam pattern, called the *decomposition layer*. The liquid foam must flow through the decomposition layer to the surface of the pattern before the gas can diffuse through the porous coating and into the sand. To sustain this motion, there must be a pressure gradient in the decomposition layer large enough to balance the viscous resistance of the liquid foam. Since the liquid metal is unable to generate this pressure gradient by itself, the metal flow front changes shape until its surface tension provides whatever pressure distribution is needed. As greater pressure gradients are required, the flow front changes from convex to concave, then to strongly concave, until at some point steady motion is no longer possible because pieces of heat-softened foam start to break off inside the concave hollow of the flow front. The metal quickly engulfs these pieces of foam and leaves them behind in its wake. When this happens, the foam stops decomposing by steady ablation, as shown in Fig. 1a, and starts to decompose by the much faster and more chaotic motion shown in Fig. 1b. This new mechanism is called *engulf mode*.

Since engulf mode involves some randomness in the way pieces of foam break free from the main body of the pattern, it is difficult to model in any deterministic way. The stable conditions leading to the *onset* of engulf mode, however, are much more tractable and probably have far more practical interest anyway. If it is possible to determine when engulf mode *begins*, then it may be possible to avoid it altogether, thereby eliminating the casting anomalies that go along with it. This is the major focus of this paper.

We begin in Section 2 by summarizing the governing equations for steady foam ablation in contact mode. In Section 3, we use data from Molibog and Littleton's [9] foam pyrolysis experiment to motivate an expression for the effective viscosity of the liquid foam in the decomposition layer. The governing equations for the equilibrium shape of the metal front are then derived in Section 4 and they are solved for a number of different cases in Section 5. These solutions involve two main nondimensional numbers that reflect the relative importance of viscosity, surface tension, and gravity. Depending on the value of these numbers, the flow front can be either convex or concave. In Section 6, we discuss the engulfing motion that sets in when the flow front becomes strongly concave, and show

how the conditions leading to such motion can be characterized by a single quantity called the *Engulf number*. In Section 7, we connect the analytical results in Section 5 with observations from numerous experiments. Finally, we discuss measures for reducing the Engulf number, including a first-ever explanation for why brominated polystyrene foams have been so successful in reducing the incidence of folds in lost foam casting of aluminum.

## 2. Foam decomposition

### 2.1. The decomposition layer

As molten aluminum fills a lost foam mold, the foam pattern normally decomposes ahead of the liquid metal by quasi-steady ablation. A narrow band of polymer liquid and gas, called the *decomposition layer*, separates the liquid metal from the solid foam. The products of the decomposing foam, are drawn though the decomposition layer (usually about 100 μm thick) as a *liquid foam* [9], until they reach the surface of the pattern, where the gas diffuses through the porous refractory coating towards the lower pressure in the sand. The small amount of residual polymer liquid that stays behind is either absorbed into the coating or simply left inside the cavity to vaporize later, after the liquid metal passes by. An idealized model of the steady foam ablation that occurs during mold filling in lost foam casting was developed in an earlier paper [8]. We begin by summarizing in this section a few of the governing equations from that model.

The decomposition layer is illustrated schematically in Fig. 2. The origin of coordinates moves with the metal front, with the $x$-axis pointing into the foam. We assume the foam decomposes at a steady velocity $u$ and the metal temperature has a uniform value $\theta_M$ on the flow front. The polymer matrix of the foam liquefies at the plane $x = l_D$, where the pattern temperature reaches a nominal "melting" temperature designated by $\theta_P$.

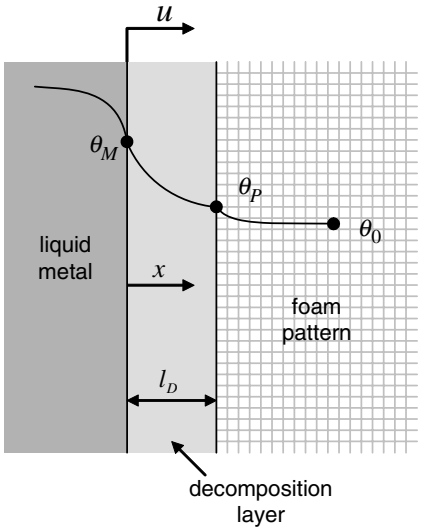


Fig. 2. Schematic illustration of the decomposition layer between the liquid metal and the receding foam.

Let $\varphi$ denote the volume fraction of air in the foam, $\rho_S$ the mass density of the solid polymer material, and $\rho_A^0$ the density of air at the initial pattern temperature $\theta_0$ and atmospheric pressure $p_0$. Then the total density $\rho_P$ of the foam pattern is given by

$$\rho_P = \varphi\rho_A^0 + (1-\varphi)\rho_S = \varphi\rho_A^0 + \rho_F, \tag{2.1}$$

where $\rho_F = (1-\varphi)\rho_S$ is the partial density of the polymer in the foam.

Let $x_V$ denote the mass fraction of the polymer material that degrades and vaporizes in the decomposition layer. The rate of vaporization $r_V$ per unit area of the metal surface can be represented quite well by an Arrhenius relationship in the form [8]

$$r_V = r_V(\theta_M, x_V) = a\exp(-E_A/R\theta_M)(1-x_V)^n, \tag{2.2}$$

where $R$ denotes the universal gas constant and the values of $a$, $E_A$, and $n$ depend on the foam material. From the definition of $x_V$ it follows that

$$x_V\rho_F u = r_V(\theta_M, x_V). \tag{2.3}$$

Unless otherwise indicated, all temperatures and pressures in this paper are taken to be absolute quantities.

Let $p_D$ denote the pressure in the decomposition layer, which we assume is independent of $x$. Let $M_V$ denote the mass-average molecular weight of the polymer vapor and $\theta_D$ the average temperature of the liquid foam. Then if we assume that the air and polymer vapor behave as ideal gases, the average mass density $\rho_D$ in the decomposition layer is given by [8]

$$\rho_D = \frac{\rho_P}{(1-x_V)(1-\varphi) + x_V\rho_F\dfrac{R\theta_D}{p_D M_V} + \varphi\dfrac{p_0\theta_D}{p_D\theta_0}}. \tag{2.4}$$

Because of the small volume fraction of liquid in the liquid foam, the first term in the denominator of (2.4) is usually negligible compared with the other two, and (2.4) may be approximated by

$$\rho_D/\rho_P = p_D/p_G, \tag{2.5}$$

where

$$p_G = (x_V\rho_F R/M_V + \varphi p_0/\theta_0)\theta_D. \tag{2.6}$$

We call $p_G$ the *gas generation pressure*. It is simply the combined pressure from the air and polymer vapor, assuming that both are contained in the same volume as the original foam.

For later reference we also define the energy per unit mass $\varepsilon_P$ required to heat the foam from its initial temperature $\theta_0$ to its "melting" temperature $\theta_P$. If we let $c_S$ denote the specific heat per unit mass of the solid polymer and $H_M$ its latent heat of fusion, then it follows that

$$\rho_P\varepsilon_P = (\varphi\rho_A^0 c_A + \rho_F c_S)(\theta_P - \theta_0) + \rho_F H_M, \tag{2.7}$$

where $c_A$ denotes the specific heat of the air in the foam. Since most foam materials are amorphous polymers, the latent heat of fusion $H_M$ is usually negligible.

### 2.2. Steady foam ablation

Let $k_D$ denote the bulk thermal conductivity of the liquid foam in the decomposition layer and $c_D$ the corresponding specific heat. Then the solution for the temperature $\theta(x)$ in the decomposition layer is [8]

$$\theta = \theta_M - \frac{\operatorname{erf}(\lambda_D x/l_D)}{\operatorname{erf}(\lambda_D)}(\theta_M - \theta_P), \tag{2.8}$$

where $\lambda_D$ is a Peclet number for the decomposition layer defined by

$$\lambda_D^2 = \frac{\rho_P c_D u l_D}{2k_D} \tag{2.9}$$

and determined by the independent equation [8]

$$\theta_M - \theta_P = \pi^{1/2}(\varepsilon_P/c_D)\lambda_D \exp(\lambda_D^2)\operatorname{erf}(\lambda_D). \tag{2.10}$$

The average temperature $\theta_D$ in the decomposition layer is given by

$$\theta_D = \frac{1}{l_D}\int_0^{l_D} \theta(x)\,\mathrm{d}x = \theta_P + (\varepsilon_P/c_D)\left[\exp(\lambda_D^2) - 1\right]. \tag{2.11}$$

Near the coating, the decomposition layer opens up into a much wider expanse, called the *coating undercut*, created by foam cells along the surface of the pattern that readily collapse because they can expel their contents directly into the adjacent coating [8]. Although the undercut controls the ultimate mold filling speed, it does not affect the shape of the metal surface, and so we do not consider it further in this paper.

The products of foam decomposition are more than 99% gas by volume. Before the metal can fill the mold, this gas must diffuse through the coating and out into the sand. For that to happen, the pressure in the decomposition layer must overcome two things: the viscous resistance of the liquid foam as it flows from the interior of the pattern towards the coating, and the resistance of the coating to gas diffusion after it gets there. Barone and Caulk [8] neglected the pressure drop in the decomposition layer, reasoning that it is almost always small compared with the pressure drop across the coating. Small or not, though, this pressure gradient still has to come from somewhere. And the only way the metal can produce it is by changing its surface curvature and relying on surface tension. It's not immediately obvious, though, that surface tension alone can produce a pressure gradient large enough to overcome the viscous resistance of the liquid foam. If it can't, then steady foam ablation may not be possible at all. We address that question more fully in this paper. First, however, we must characterize the viscous resistance of the liquid foam.

## 3. Effective viscosity of the liquid foam

### 3.1. Steady foam pyrolysis

Molibog and Littleton [9,10] developed a foam pyrolysis apparatus that simulates the interaction between a foam pattern and liquid metal in lost foam casting. The apparatus pushes a long foam bar through an electrically heated metal strip at a constant velocity. The metal strip is maintained at a constant temperature by regulating its power input. Gas fraction and heat flux measurements were considered in an earlier paper [8]. Here we focus on the measurements of the load exerted on the end of the foam bar.

Molibog and Littleton [9] pyrolyzed three lost foam grade polystyrene foam materials at nominal velocities of 1, 3, and 4.5 cm/s. After correcting for the friction between the foam bar and the metal rails that guide the bar into the heater, the experimenters converted the measured load to an average pressure exerted by the foam bar on the surface of the heated metal strip. Fig. 3 shows a plot of the measured pressure as a function of heater temperature for one of those materials (StyroChem T170B with a nominal density of 25 kg/m$^3$) at all three speeds. Each symbol on these graphs represents a measurement from a single foam bar. The pressure drops exponentially with increasing temperature and it grows quite rapidly with increasing speed. At the slowest speed, the measured pressures were close in value to the estimated friction forces (equivalent to about 400 Pa on the heater), which is probably responsible for the large scatter in the results for the 1 cm/s speed, especially at the higher heater temperatures.

### 3.2. Lubrication theory

Even though the liquid foam in the decomposition layer is not really a homogeneous Newtonian fluid, it is still instructive to apply lubrication theory to the squeezing motion of the decomposition products in the narrow gap

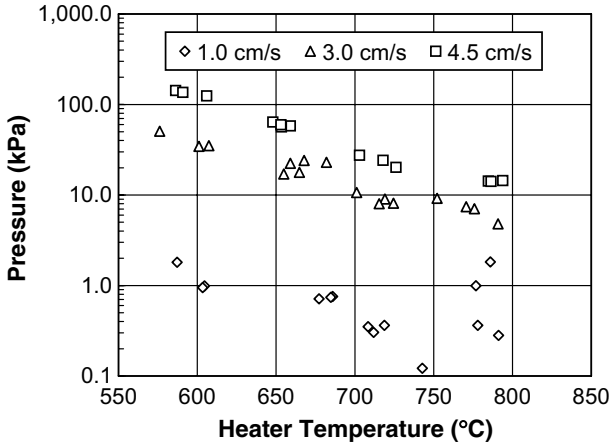


Fig. 3. Average pressure on the metal heater during pyrolysis of a polystyrene foam bar, measured by Molibog and Littleton [9] as a function heater temperature for three different speeds.

between the heater and the unmelted foam to derive an expression relating pressure, speed, and apparent viscosity of the liquid foam. We can then compare this relationship with the experimental data in Fig. 3 and use the solution in (2.10) and (2.11) to see how the apparent viscosity of the liquid foam depends on the average temperature in the decomposition layer.

The geometry of the heater and pyrolyzing foam is shown in Fig. 4. Let $y$ measure the distance away from the center of the heater and $d$ the overall heater width. If we assume two-dimensional flow and adopt the usual assumptions of lubrication theory, then the velocity $v$ in the liquid foam between the heater and the unmelted foam is given by

$$v(x,y) = -\frac{l_D^2}{2\mu_D}\frac{\mathrm{d}p_D}{\mathrm{d}y}\frac{x}{l_D}(1 - x/l_D), \tag{3.1}$$

where $\mu_D$ denotes the effective viscosity of the liquid foam. Integrating (3.1) across the thickness of the decomposition layer, we obtain

$$l_D v_A(y) = \int_0^{l_D} v(x,y)\,\mathrm{d}x = -\frac{1}{12}\frac{l_D^3}{\mu_D}\frac{\mathrm{d}p_D}{\mathrm{d}y}, \tag{3.2}$$

where $v_A(y)$ is the average velocity of the liquid foam at the position $y$. For mass to be conserved we must have

$$\rho_D l_D v_A = \rho_P u y, \tag{3.3}$$

and so with (3.2) the pressure gradient is given by the simple expression

$$\rho_D\frac{\mathrm{d}p_D}{\mathrm{d}y} = -12\mu_D\frac{\rho_P u y}{l_D^3}. \tag{3.4}$$

Substituting (2.5) into (3.4) and integrating with respect to $y$, we obtain

$$p_D^2 - p_0^2 = 3\mu_D\frac{p_G u d^2}{l_D^3}\left[1 - \left(\frac{2y}{d}\right)^2\right], \tag{3.5}$$

where $p_0$ is the atmospheric pressure. The average pressure over the heater width is then

$$p_A = \frac{1}{d}\int_{-d/2}^{d/2} p_D\,\mathrm{d}y = \frac{1}{2}p_0\left[1 + \omega^{1/2}(\omega^{-1}+1)\sin^{-1}(\omega^{-1}+1)^{-1/2}\right], \tag{3.6}$$

where $\omega$ is a nondimensional quantity defined by

$$\omega = 3\mu_D\frac{p_G u d^2}{p_0^2 l_D^3}. \tag{3.7}$$

### 3.3. Effective viscosity

The heater width $d$, the velocity $u$, and the foam density $\rho_F$ are all prescribed quantities, the average pressure $p_A$ is measured in the experiment, and the pressure $p_G$ and layer thickness $l_D$ depend on the heater temperature through the heat conduction solution (2.8). A table of material properties for this foam material is given in [8]. We can then use (3.6) and (3.7) to express the viscosity $\mu_D$ as a function of the average temperature in the decomposition layer. This result is plotted in Fig. 5. Most of the data clusters around a straight line on this semi-log plot, suggesting a relationship for viscosity in the form

$$\mu_D = \mu_0\exp(-A\theta_D) \tag{3.8}$$

and lending some validity to the use of lubrication theory in this context. The straight line superimposed on the data in Fig. 5 represents the best linear fit to the experimental data, excluding the erratic measurements above 700 °C for the 1 cm/s speed, which were not much larger than the correction for friction, anyway. The best-fit viscosity coefficients from (3.8) corresponding to the straight line in Fig. 5 are

$$\mu_0 = 1.1\times 10^8\ \text{Pa s}, \quad A = 0.042\ \text{K}^{-1}. \tag{3.9}$$

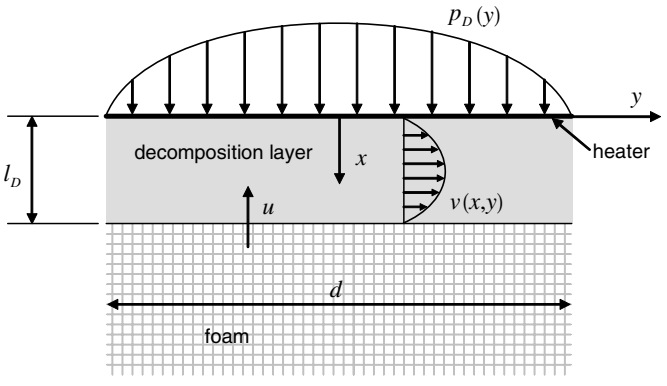


Fig. 4. Geometry and coordinates for analysis of the pressure load on the metal heater during pyrolysis of foam bars.

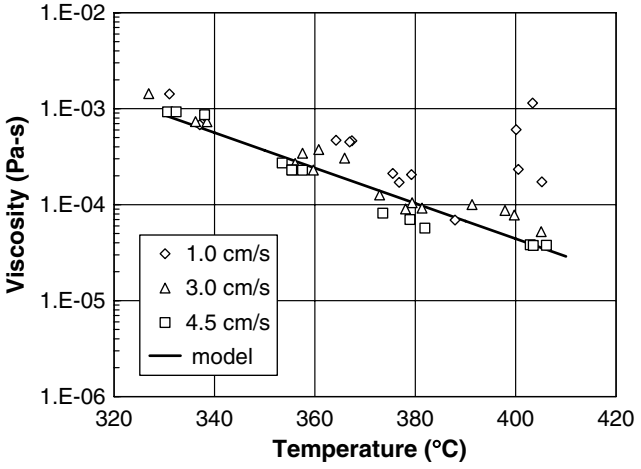


Fig. 5. Apparent viscosity of liquid foam in the decomposition layer for polystyrene foam, calculated from (3.6) and (3.7) as a function of the average temperature in the decomposition layer for three different speeds. The solid line represents the best fit with the temperature dependence expressed by (3.8).

Although the solution (3.6) and (3.7) could be used to correct the results in [8] by computing an explicit pressure drop in the decomposition layer, the difference turns out to be fairly small. The real utility of these results is in determining the equilibrium shape of the metal front.

## 4. Metal surface equilibrium

### 4.1. Geometry and kinematics

In the previous section, we used lubrication theory to calculate the pressure distribution required to force the liquid foam through the decomposition layer, assuming that the flow front was plane. While that assumption is certainly appropriate for the metal heater in Molibog and Littleton's [9,10] foam pyrolysis experiments, it may not be true for the liquid metal in the actual casting process. That's because the nearly rigid metal heater in the experiment is able to support whatever pressure gradient is needed without changing shape, but the liquid metal cannot. We reconsider that analysis in this section, but this time allow the metal front to assume whatever shape it needs for surface tension on the liquid metal to balance the viscous resistance of the liquid foam.

Consider steady, two-dimensional foam decomposition in a pattern of uniform thickness $d$. Let $x$ and $y$ denote fixed rectangular Cartesian coordinates such that $y$ measures the transverse distance from the mid-plane of the pattern and $x$ points in the direction of flow (see Fig. 6). Let $\mathbf{r}(x,y,t)$ denote the position vector to any point on the metal surface at time $t$. Then if the entire flow front moves ahead with steady velocity $u$, we can set

$$\mathbf{r} = \mathbf{r}(y,t) = [ut + r(y)]\mathbf{e}_1 + y\mathbf{e}_2, \tag{4.1}$$

where $\mathbf{e}_1$ and $\mathbf{e}_2$ are the unit Cartesian base vectors and $r(y)$ measures the deviation of metal surface from plane. Without loss in generality, we take

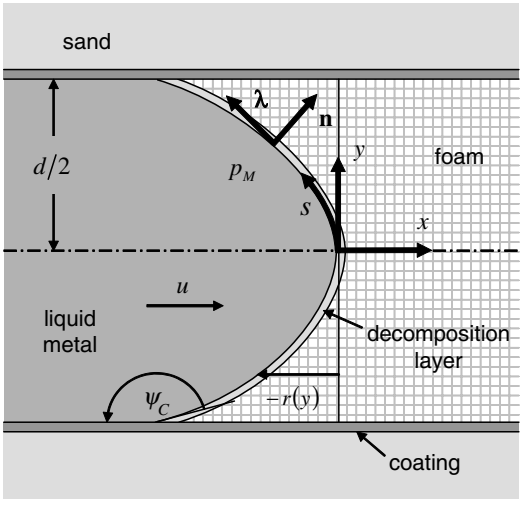


Fig. 6. Geometry and coordinates on the metal flow front through a section of the cavity.

$$r(0) = 0. \tag{4.2}$$

Now let $s$ measure arc length along the flow front, starting from $y = 0$. Then from (4.1)

$$\mathrm{d}s^2 = \mathrm{d}\mathbf{r}\cdot\mathrm{d}\mathbf{r} = (1 + r'^2)\,\mathrm{d}y^2 \tag{4.3}$$

and so

$$\mathrm{d}s = \sqrt{1 + r'^2}\,\mathrm{d}y, \tag{4.4}$$

where a prime denotes differentiation with respect to $y$. The unit tangent $\boldsymbol{\lambda}$ to the flow front is given by

$$\boldsymbol{\lambda} = \frac{\mathbf{r}'}{|\mathbf{r}'|} = \frac{r'\mathbf{e}_1 + \mathbf{e}_2}{\sqrt{1 + r'^2}} \tag{4.5}$$

and the outward unit normal $\mathbf{n}$ by

$$\mathbf{n} = \frac{\mathbf{e}_1 - r'\mathbf{e}_2}{\sqrt{1 + r'^2}}. \tag{4.6}$$

The local curvature $\kappa$ of the flow front (defined by $\partial\boldsymbol{\lambda}/\partial s = \kappa\mathbf{n}$) is then

$$\kappa = \frac{r''}{(1 + r'^2)^{3/2}}. \tag{4.7}$$

Since the flow front is a material surface,

$$\begin{aligned}\frac{\mathrm{d}}{\mathrm{d}t}[x - ut - r(y)] &= \dot{x} - u - r'\dot{y} \\ &= -u + \sqrt{1 + r'^2}(\dot{\mathbf{r}}\cdot\mathbf{n}) = 0.\end{aligned} \tag{4.8}$$

It follows that the normal velocity of the metal surface at any point along the flow front is given by

$$u_n = \dot{\mathbf{r}}\cdot\mathbf{n} = \frac{u}{\sqrt{1 + r'^2}}. \tag{4.9}$$

### 4.2. Balance of mass and momentum

By analogy to (3.2), the volume flow rate $Q(s)$ of liquid foam though the decomposition layer is related to the tangential pressure gradient by

$$Q(s) = -\frac{1}{12}\frac{l_D^3}{\mu_D}\frac{\mathrm{d}p_D}{\mathrm{d}s} = -\frac{1}{12}\frac{l_D^3}{\mu_D}\frac{1}{\sqrt{1 + r'^2}}\frac{\mathrm{d}p_D}{\mathrm{d}y}, \tag{4.10}$$

where $l_D(y)$ now represents the *normal* thickness of the decomposition layer. Since the foam mass must be conserved, the volume flow rate at any point $s$ is related to the forward metal velocity by

$$\rho_P u y = \rho_D Q = \frac{p_D}{p_G}\rho_P Q, \tag{4.11}$$

where we have used (2.5).

According to (2.10), the Peclet number $\lambda_D$ in the decomposition layer depends solely on the temperature of the liquid metal. For simplicity we assume that the metal temperature is uniform through the section thickness, so that $\lambda_D$ is also uniform. Then from (2.9) and the expression for the normal velocity (4.9), the thickness of the decomposition layer is given by

$$l_D(y) = \frac{2k_D\lambda_D^2}{\rho_P c_D u_n} = \frac{2k_D\lambda_D^2}{\rho_P c_D u}\sqrt{1+r'^2}. \tag{4.12}$$

Note that decomposition layer begins to vary in thickness as soon as the flow front assumes any non-planar shape, i.e., $r' \neq 0$. Combining Eqs. (4.10)–(4.12), we obtain

$$p_D\frac{\mathrm{d}p_D}{\mathrm{d}y} = -\frac{3}{2}\mu_D p_G u^4\left(\frac{\rho_P c_D}{k_D\lambda_D^2}\right)^3\frac{y}{1+r'^2}. \tag{4.13}$$

This equation expresses the local balance of momentum in a non-planar decomposition layer. It is interesting to note from (4.13) that even though the liquid foam has to flow *farther* to reach the coating in a curved decomposition layer, the pressure drop required to get it there actually *decreases*.

### 4.3. Surface tension

Since normal filling speeds in lost foam casting are relatively slow (1–2 cm/s), the dynamic pressure in the liquid metal is negligible compared with its static pressure due to gravity. Let $p_M$ denote the metal pressure at the flow front and $p_M^0$ the pressure at $y = 0$. Further, let $g$ denote the acceleration of gravity, $\rho_M$ the density of the liquid metal, and $\mathbf{k}$ the unit vector pointing vertically upward. Then the pressure in the metal at any point on the flow front is given by

$$\begin{aligned} p_M(y) &= p_M^0 - \rho_M g\mathbf{k}\cdot[\mathbf{r}(y,t) - \mathbf{r}(0,t)] \\ &= \rho_M g(H_0 - rk_1 - yk_2), \end{aligned} \tag{4.14}$$

where

$$\mathbf{k} = k_1\mathbf{e}_1 + k_2\mathbf{e}_2 \tag{4.15}$$

and

$$H_0 = p_M^0/\rho_M g \tag{4.16}$$

is the metal head at $y = 0$.

Quasi-static pressure equilibrium between the liquid metal and the decomposition layer requires that

$$\tau\kappa = p_D - p_M = p_D - \rho_M g(H_0 - rk_1 - yk_2), \tag{4.17}$$

where $\tau$ denotes the constant surface tension of the liquid metal and $\kappa$ is the local curvature of the metal surface defined by (4.7). Combination of (4.13) and (4.17) yields

$$\begin{aligned} &[\tau\kappa + \rho_M g(H_0 - rk_1 - yk_2)][\tau\kappa' - \rho_M g(k_1 r' + k_2)] \\ &\quad = -\frac{3}{2}\mu_D p_G u^4\left(\frac{\rho_P c_D}{k_D\lambda_D^2}\right)^3\frac{y}{1+r'^2}. \end{aligned} \tag{4.18}$$

Together with the definition of the curvature in (4.7), this is a third-order, nonlinear ordinary differential equation for the surface profile $r(y)$. Eq. (4.2) provides one boundary condition. The other two depend on the contact angle $\psi_C$ between the liquid metal and the coating at the boundary of the cavity, i.e.,

$$\tan^{-1} r'(\pm d/2) = \pm\psi_C. \tag{4.19}$$

### 4.4. Nondimensional equations

The governing equations for the shape of the metal front can be expressed in a more revealing form by changing to nondimensional variables. Suppose we divide both $y$ and $r$ by the half-thickness of the cavity, $d/2$, but still use the same symbols for both nondimensional quantities. Then (4.18) may be written as

$$[1 + D(\kappa/G - rk_1 - yk_2)][\kappa' - G(k_1 r' + k_2)] = -P\frac{y}{1+r'^2}, \tag{4.20}$$

where $\kappa$ now represents a nondimensional curvature and $P$, $D$, and $G$ are dimensionless numbers defined by

$$D = \frac{d}{2H_0}, \qquad G = \frac{\rho_M g d^2}{4\tau}, \quad P = \frac{3}{2}\frac{\mu_D p_G u^4}{\tau p_M^0}\left(\frac{\rho_P c_D d}{2k_D\lambda_D^2}\right)^3. \tag{4.21}$$

The boundary condition (4.2) is unchanged, and (4.19) becomes

$$\tan^{-1} r'(\pm 1) = \pm\psi_C. \tag{4.22}$$

The nondimensional number $D$ measures the thickness of the pattern compared with the head of liquid metal. Since $D$ is typically about $10^{-2}$ and $G = \mathrm{O}(1)$, we can usually approximate (4.20) by the much simpler expression

$$\kappa' - G(k_1 r' + k_2) = -P\frac{y}{1+r'^2}. \tag{4.23}$$

The two remaining nondimensional numbers measure the relative significance of the three main forces that shape the flow front: (1) viscosity of the liquid foam, (2) surface tension of the liquid metal, and (3) gravity. The dimensionless quantity $G$ measures the ratio of gravity to surface tension forces, while $P$ measures the ratio of viscous to surface tension forces. Since both numbers are usually order 1 or larger, the gravitational, viscous, and surface tension forces are more-or-less equally balanced. It is likely, then, that by changing the process variables even a little bit, we may see the shape of the flow front alter a great deal, especially since $P$ depends on some variables to the third and fourth powers. We call $P$ the *Profile number*. For a given metal, $G$ depends only on the pattern thickness. For certain orientations of the pattern and flow direction relative to gravity (expressed by the values of $k_1$ and $k_2$), $G$ may not enter the governing Eq. (4.23) at all. When it does, it usually varies over a much narrower range than $P$. Hence the Profile number is the dominant parameter affecting the shape of the flow front. In the next section, we consider numerical solutions of (4.23) under a variety of process conditions.

### 4.5. Limiting case

Before we solve (4.23) under more general conditions, however, it is instructive to consider a special case where this equation has an analytical solution. Suppose the pat-

tern is oriented vertically and the flow front is moving horizontally. Then $k_1 = k_2 = 0$. Suppose further that the liquid foam has a negligible viscosity. Then $P$ vanishes, and the governing Eq. (4.23) reduces to

$$\kappa' = 0, \tag{4.24}$$

and so the flow front must have a uniform curvature. Since the contact angle for aluminum on a refractory material is usually greater than 90°, the flow front must assume a *convex* shape in the form of a circular arc of (nondimensional) radius $r_0$. The solution for $r(y)$ is

$$r(y) = \sqrt{r_0^2 - y^2} - r_0. \tag{4.25}$$

The value of $r_0$ depends on the contact angle $\psi_C$. Aluminum alloys have a contact angle of about $3\pi/4$ radians on most coating substrates. Hence the nondimensional boundary condition corresponding to (4.22) becomes

$$r'(\pm 1) = \mp 1. \tag{4.26}$$

When this condition is imposed on (4.25), we find that $r_0 = \sqrt{2}$. Hence the radius of curvature of the flow front is about 70% of the local pattern thickness.

Even though the viscosity of the liquid foam is never really zero, its effect on the solution may be indeed negligible if the section thickness and filling speeds are both small enough to make $P \ll 1$. Molten aluminum has a surface tension of about 1 N/m. From the properties of polystyrene foam tabulated in [8] and the liquid foam viscosity plotted in Fig. 5, it's easy to show that $P \ll 1$ as long as the pattern is less than 5 mm thick and the mold filling speed is about 1 cm/s. Hence the simple convex solution (4.25) should represent the actual flow front geometry in thin parts that fill slowly.

## 5. The shape of the metal front

### 5.1. Four special cases

The solution of the differential equation (4.23) for the shape of the flow front depends on the two direction cosines $k_1$ and $k_2$. The first of these measures the orientation of the gravity direction **k** relative to the direction of flow and the second its orientation relative to plane of the pattern. Out of the infinity of possibilities represented by these two parameters, we consider only four specific cases in this paper. They are

| | |
|---|---|
| 1. Vertical pattern filling from the side | $k_1 = 0, k_2 = 0$ |
| 2. Horizontal pattern | $k_1 = 0, k_2 = 1$ |
| 3. Vertical pattern filling from the bottom | $k_1 = 1, k_2 = 0$ |
| 4. Vertical pattern filling from the top | $k_1 = -1, k_2 = 0$ |

It should be possible to infer the general behavior of most other situations from these four special cases.

In all cases, we solved the nonlinear differential equation (4.23) subject to the three boundary conditions (4.2) and (4.26), using a standard forward difference scheme, starting at one end of the profile and iterating on the beginning curvature until the boundary condition (4.26) was satisfied on the other end.

### 5.2. Vertical pattern filling from the side

In this case, the metal pressure is independent of $y$, and $G$ drops out of the governing Eq. (4.23). Fig. 7 displays the resulting surface profiles for four different values of $P$ between 0 and 100. The flow front profile, which is symmetric about $y = 0$, is identical to the convex analytical solution in the previous section when $P = 0$. It flattens out at higher values of $P$ until it becomes almost plane near $P = 10$, and then it grows increasingly concave for values higher than that. This happens because the surface curvature must decrease with $y$ to create a negative pressure gradient in the decomposition layer. A greater pressure gradient is required for larger values of $P$, and so the curvature has to begin at increasingly higher values in the center of the pattern. Eventually this creates a strongly concave flow front.

Fig. 8 shows how the pressure gradient (normalized by $4\tau/d^2$) varies across the thickness of the pattern for the same values of $P$. The pressure gradient is highest near the coating where the velocity of the liquid foam is the greatest. It dips to a local minimum about halfway between the center of the pattern and the boundary because at this point the profile achieves its maximum slope (Fig. 7) and the normal thickness $l_D$ of the decomposition layer also reaches a maximum (Fig. 9). As the decomposition layer gets thicker, the viscous resistance drops and the local pressure gradient decreases. At larger values of $P$, $l_D$ grows to several times its value in the center of the pattern because of the steepening slope of the flow front (see Eq. (4.12)).

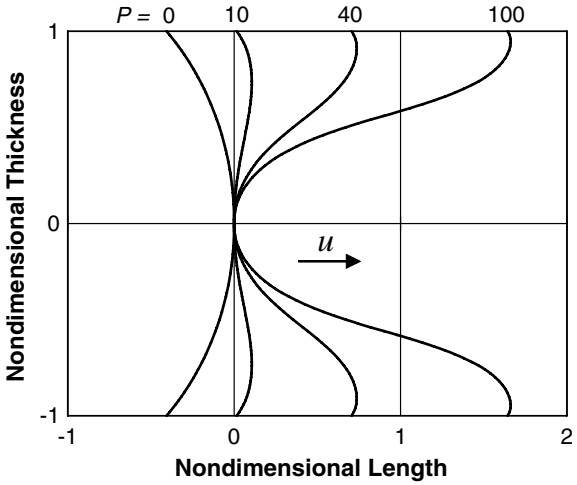


Fig. 7. Flow front profiles for a vertical pattern filling from the side, computed for four values of the Profile number $P$.

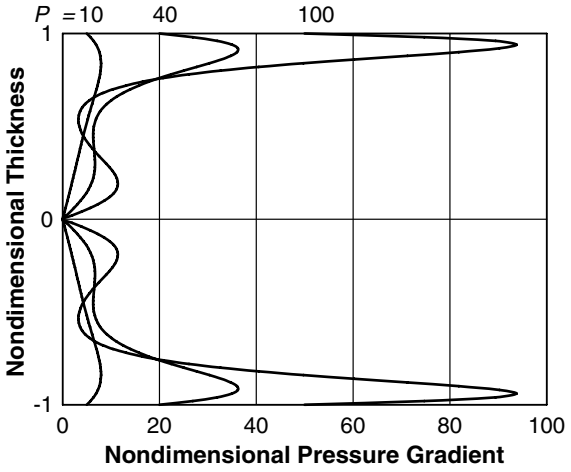


Fig. 8. Magnitude of the pressure gradient in the decomposition layer (normalized by $4\tau/d^2$) as a function of location through the pattern thickness for a vertical pattern filling from the side, computed for three values of the Profile number $P$.

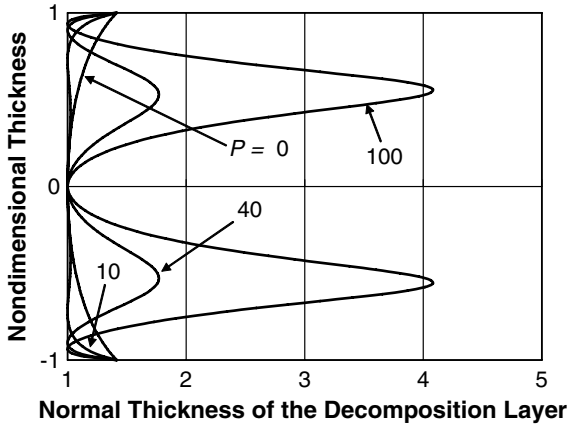


Fig. 9. Normal thickness of the decomposition layer (divided by its value in the center of the pattern) as a function of location through the pattern thickness for a vertical pattern filling from the side, computed for four values of the Profile number $P$.

### 5.3. Horizontal pattern

In this case, gravity acts across the pattern thickness, creating a metal pressure that increases from top to bottom. Fig. 10 displays the corresponding flow front profiles calculated for $G = 1$ and the same four values of $P$. For molten aluminum, $G = 1$ corresponds to a pattern thickness of about 12 mm. The variation in metal pressure upsets the symmetry of the previous solution, skewing the profile across the pattern thickness. The pressure gradient in the liquid metal opposes the movement of liquid foam towards the bottom of the pattern and assists it towards the top. Hence the change in curvature must be greater for $y < 0$ than it is for $y > 0$. This causes the bottom of the profile to be more concave than the top and the bottom edge of the flow front to lead the top edge. Larger values of $G$ (thicker patterns) skew the profile even more. The general trend towards a more concave profile at increasing values of $P$ continues to hold in this case just as it did in Fig. 7. The pressure gradients for this case are only slightly skewed from those in Fig. 8, and so we do not show them here.

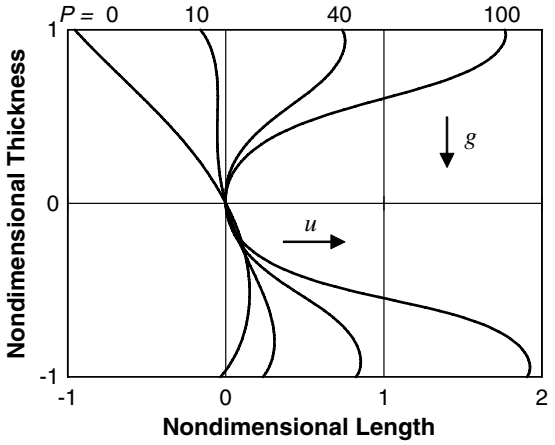


Fig. 10. Flow front profiles for a horizontal pattern, computed for four values of the Profile number $P$.

### 5.4. Vertical pattern filling from the bottom

In this case, gravity acts against the direction of flow, creating a positive pressure gradient in the liquid metal from the leading towards the trailing edge of the flow front. Fig. 11 shows the flow front profiles calculated for $G = 1$ and the same values of $P$ as before. The flow front profiles, which again are symmetric about $y = 0$, are similar to those in Fig. 7, except that for the same value of $P$, the convex flow fronts are less convex and the concave flow fronts are less concave. This is because the pressure gradient in the liquid metal opposes the movement of liquid foam

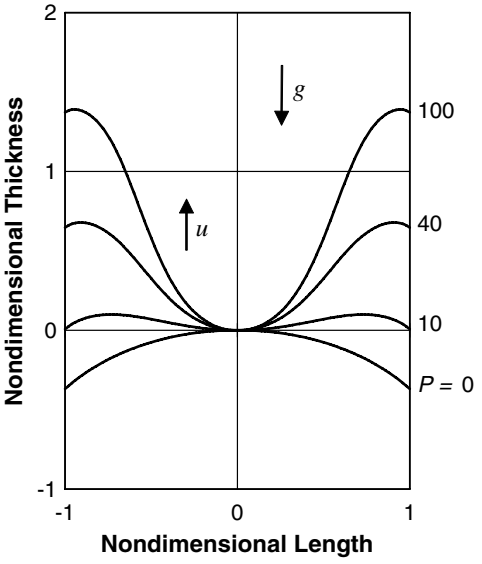


Fig. 11. Flow front profiles for a vertical pattern filling from the bottom, computed for four values of the Profile number $P$.

towards the sides of the pattern when the flow front is convex and assists when it is concave. The net effect is to draw the cluster of profiles closer together. At higher values of $G$ (thicker patterns), they grow closer still. The pressure gradients for this case are nearly identical to those in Fig. 8, and so we do not show them here.

### 5.5. Vertical pattern filling from the top

In this case, gravity acts in the same direction as the flow, so that the metal pressure is highest at the leading edge of the flow front. Fig. 12 shows the flow front profiles calculated for $G = 1$ and four values of $P$ from 0 to 65. Again, the profiles are symmetric about $y = 0$ and similar in shape to those in Figs. 7 and 11. In this case, though, the convex profiles are more convex for the same value of $P$ and the concave profiles are more concave. This time the pressure gradient in the liquid metal opposes the movement of the liquid foam when the flow front is concave and assists it when it is convex. Instead of gravity drawing the profiles closer together as it did when filling from the bottom, in this case it spreads them out. The profiles spread even farther apart at larger values of $G$ (thicker patterns).

The big difference in this case, though, is that for values of $P$ slightly greater than 65 no steady solution exists at all. Here the outward pressure gradient produced in the decomposition layer by surface tension on the increasingly concave flow front is offset by an opposing pressure gradient in the liquid metal due to the corresponding change in surface elevation. Eventually, gravity outstrips surface tension and the pressure gradient in the decomposition layer drops to zero somewhere between the center and the boundary of the pattern, stopping the flow of decomposition products towards the coating. This trend is clearly evident in the results for the pressure gradient shown in Fig. 13. When the Profile number is larger than about 65, the flow front does not approach a steady shape at all. Instead, the outer lobes continue down the sides of the pattern, leaving behind a core of undecomposed foam in the center. As $G$ gets larger (the pattern gets thicker), a steady solution exists for an ever-decreasing range of $P$.

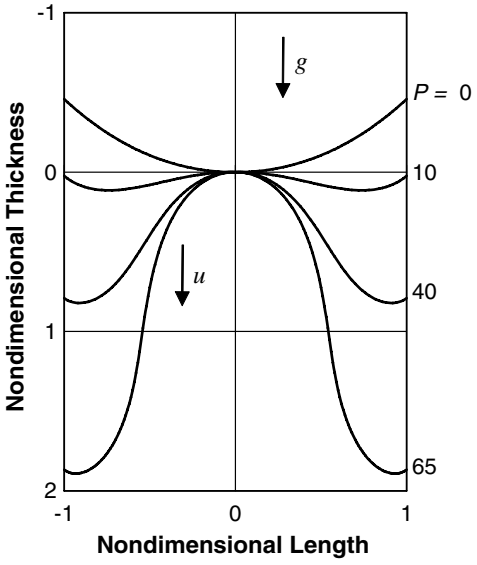


Fig. 12. Flow front profiles for a vertical pattern filling from the top, computed for four values of the Profile number $P$.

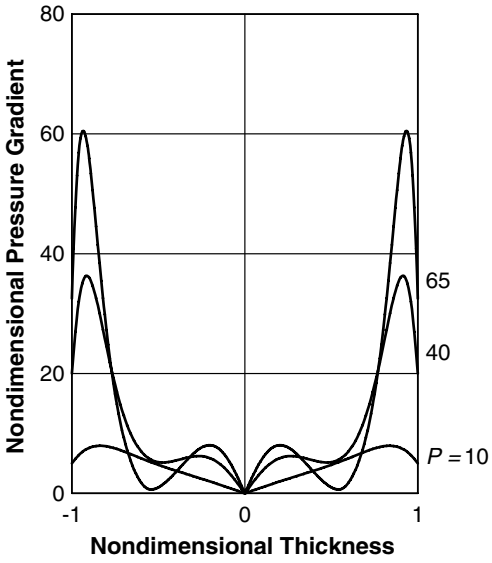


Fig. 13. Magnitude of the pressure gradient in the decomposition layer (normalized by $4\tau/d^2$) as a function of location through the pattern thickness for a vertical pattern filling from the top, computed for three values of the Profile number $P$.

For similar reasons, the steady solution in the horizontal pattern (Fig. 10) exists only for $P < 150$. As we shall see in the next section, though, unsteady engulfing motion may set in before that limit is ever reached.

## 6. Engulfing motion

### 6.1. Foam encirclement

Regardless of the orientation of gravity, the results of the previous section show that the flow front becomes increasingly concave as the Profile number $P$ increases. Eventually, the metal surrounds a narrow core of foam on two sides, as depicted schematically in Fig. 14. If there is a sudden perturbation in the flow or a random flaw in the foam, some part of this foam core, already softened somewhat by the heat of the liquid metal, may suddenly break off from the main body of the pattern. When this happens, the metal encircles the broken piece of foam, causing it to liquefy very quickly and then vaporize. Since the polymer vapor is unable to escape, it forms a relatively large bubble inside the metal stream that should continue to contain residual liquid for some time. These are the same bubbles that appear in the X-ray images in Fig. 1b. Since the bubbles have the same light intensity on the X-ray as the original foam, they probably extend through the entire thickness of the pattern. Once such bubbles form, they

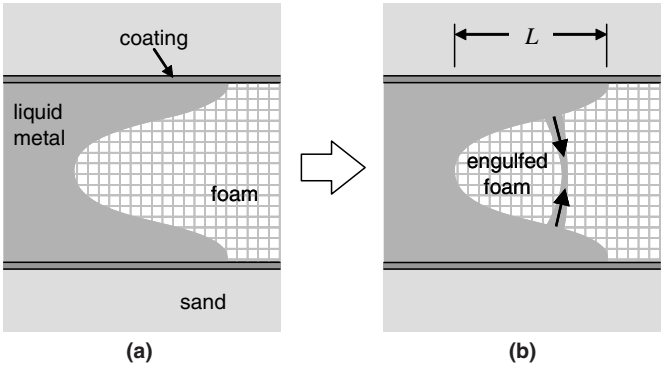


Fig. 14. Development of a foam core inside the hollow of a concave flow front before (a) and after (b) the foam core breaks off, allowing the metal to engulf a piece of the foam.

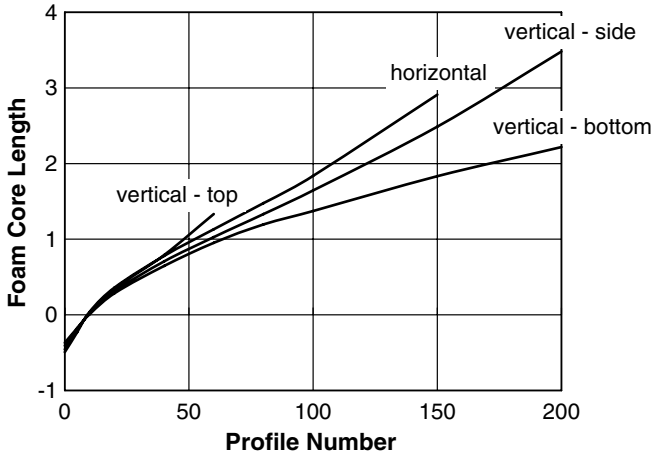


Fig. 15. Nondimensional foam core length $r(1)$ as a function of $P$ for four different pattern/flow orientations relative to gravity.

may rise to the top of the liquid metal or lodge somewhere in the mold cavity. Either way, they are likely to cause anomalies in the casting if they do not dissipate before the metal solidifies. And even when they do dissipate, their oxide-covered surfaces may not be able to fuse, leaving a fold in the casting.

Although the actual process of foam encirclement and bubble formation may be too complex to model explicitly, we still should be able to use the analysis of the previous section to come up with a reasonable estimate of when it *begins*. To do that, we consider how the geometry of the foam core affects the stresses that arise from unbalanced loads that may act on it.

### 6.2. Engulf number

Consider a foam core of length $L$ between the two lobes of metal as illustrated in Fig. 14. If we regard the foam core as a cantilever beam, then the maximum stress created by a transverse load on the free end is proportional to $L/d^2$. From the previous section we have

$$L = r(1)d/2. \tag{6.1}$$

Fig. 15 shows how $r(1)$ depends on the Profile number $P$ for each of the four cases considered in the previous section (for the horizontal pattern, we plot the average of the two lobes). For $P > 20$ (after the flow front becomes concave), the dependence is very nearly linear in all cases. Hence $L$ is roughly proportional to $Pd$, and the maximum stress should be proportional to $P/d$.

With this as motivation, we propose the following measure, called the *Engulf number*, for indicating when engulfing motion begins:

$$E = \frac{\mu_D p_G u^4 d^2}{\tau p_M^0}\left(\frac{\rho_P c_D}{k_D \lambda_D^2}\right)^3. \tag{6.2}$$

When the Engulf number becomes sufficiently large, the steady process of foam decomposition starts to break down and the metal begins to envelop pieces of the foam pattern. But since we are unable estimate the strength of the foam core or know what loads are likely to act on it, it's impossible to say at this point how large the "critical" Engulf number should be.

### 6.3. Engulf mode

After the metal engulfs a piece of the foam pattern, the flow front should flatten out somewhat before it starts to redevelop a concave shape. This creates a pseudo-periodic foam decomposition process in which the metal engulfs a piece of foam, the concave flow front develops anew, and foam is encircled again. We call this process *engulf mode*. Engulf mode should appear to progress in a pulse-like manner, something that at least one group of experimenters claim to have observed [6].

Analyzing the unsteady, pulsing motion of engulf mode is sure to be difficult if it is possible at all, and we do not attempt it here. But it is worth remarking on the effect that the resulting gas bubbles may have on the continuing process of foam decomposition. In a vertical pattern filling from the top, for example, bubbles are shed above and behind the flow front, so they shouldn't interfere with subsequent foam decomposition. On the other hand, for a vertical pattern filling from the bottom, the bubbles should stay with the flow front, which may trigger the onset of *gap mode* [11]. For a vertical pattern filling from the side (Fig. 1 provides a good example), the bubbles rise more or less parallel to the flow front, so they shouldn't interfere with continuing foam decomposition much at all.

## 7. Experimental observations

The analysis in the previous two sections helps to explain a variety of experimental observations about lost foam casting that up to now have not been well understood. These observations come from experiments that fall into two main categories: (1) mold filling studies that reveal

the shape and dynamics of the metal flow front, and (2) casting anomaly investigations that show how the incidence of porosity, folds, and blisters depends on different process variables. Since engulf mode is probably responsible for creating many of the fill-related anomalies in lost foam casting of aluminum, the anomaly studies deserve special attention, not just because they confirm many of the theoretical results, but also because they can be used together with the model to suggest ways of avoiding engulf mode altogether.

### 7.1. Mold filling

The X-ray images taken by Sun et al. [5]—one of which is reproduced here in Fig. 1—are probably the best available direct evidence of engulf mode, especially when they are viewed in full motion video. The large bubbles forming along the flow front in these images are undoubtedly caused by polymer that gets trapped inside the metal and then rapidly vaporizes. This is evident not only from the size of the bubbles themselves, but also from how long they maintain their size even after their gas begins to diffuse through the coating and into the sand. Evidently, continued vaporization of the remaining polymer liquid inside the bubbles replenishes the gas lost through the coating. Although there are bubbles scattered throughout the metal in the still image in Fig. 1b, all of them originally formed just behind the metal front and then either stayed in place as the metal moved forward or drifted upwards as the mold filled. This suggests that metal envelops the foam material near the flow front rather than sometime later after the metal front passes by.

In a relatively early study, Katashima et al. [12] stopped the liquid metal part way through mold filling by using a vacuum to draw water into the sand. Although this unusual quenching process may alter the filling pattern somewhat just before the metal freezes, the shape of the solidified metal should still provide a reasonably accurate picture of the actual flow front geometry. In any case, these authors found a dramatic difference in the filling pattern depending on whether or not metal fill was accelerated by drawing a vacuum on the sand as the mold filled. Without a vacuum, the mold filled slowly and the flow front was convex, but with a vacuum (as high as 0.4 atmospheres) the metal flowed rapidly and preferentially along the coated surface of the pattern, surrounding a core of foam in the interior. In the first case, the flow front was convex and the decomposition products were swept to the boundary. In the second, the metal flowed ahead along the coating and then encircled the foam in the interior of the pattern. This is strong evidence that engulfing motion is brought on by rapid filling speeds. Note too that these authors observed metal flowing long distances along the coating before the foam core decomposed. This may be evidence for the unsteady motion discussed in Section 5 that sets in for top-filling patterns at high values of the Profile number $P$.

More recently, Liu et al. [13] observed similar mold filling behavior in a magnesium alloy. These authors found that when they applied a vacuum (this time as high as 0.5 atmospheres) on the mold to increase the filling speed, the metal flowed "preferentially against the pattern wall" and, "meet[ing] in the central pattern ahead of the metal front," enclosed pieces of the pattern, creating bubbles. This anecdotal evidence also supports the existence of the engulfing motion described in Sections 5 and 6.

Using embedded thermocouples in foam bars cast horizontally, Miller [3] and Warner et al. [14] found that as coating permeability increased, filling speeds also increased and the shape of the flow front grew increasingly concave. These trends were also accompanied by growing number of casting anomalies in the form of porosity, folds, and blisters. Sun et al. [15], also using embedded thermocouples, observed flow front profiles in cylindrical patterns cast horizontally. With a low permeability coating these authors saw a profile that looked similar to the curve for $P = 0$ in Fig. 7 and with a higher permeability, they saw a flatter profile similar to the one for $P = 10$. As the coating permeability increases, the filling speed also increases [8], and this leads to higher values of $P$, consistent with these results.

### 7.2. Casting anomalies

From the earliest studies on lost foam casting, researchers have suspected that fill-related casting anomalies were caused by partially decomposed foam that gets trapped inside the liquid metal. There is no agreement, though, on how or why this occurs. In the last several years, systematic experiments have revealed definite relationships between fill-related casting anomalies and certain process variables. For the most part these studies have concentrated on porosity, folds, and blisters, reasoning that because these anomalies usually contain trace amounts of carbon, they must be caused by entrapped foam. If it is true that engulf mode is the main cause of the casting anomalies observed in these studies, then each trend that leads to more anomalies should also increase the Engulf number (4.2).

Nearly all investigators identify filling speed as the dominant variable affecting casting anomalies. Wang et al. [16], Miller [3], Sun et al. [15], Hill et al. [17], and Tschopp et al. [18] all found that higher filling speeds led to more blisters, folds, and porosity. Since the Engulf number (4.2) depends on filling speed to the fourth power, any process change that increases filling speed—even just a little—increases the Engulf number significantly.

Miller [3] and Bennett et al. [19] both found that the number of anomalies increased with section thickness. This is consistent with the fact that the Engulf number is proportional to $d^2$. While section thickness does not affect the Engulf number as much as filling speed, it is still an important variable.

Wang et al. [16], Sun et al. [15], Hill et al. [17,7], and Bennett et al. [19] all found that by raising metal temperature

they could reduce the number and severity of casting anomalies. Although metal temperature does not appear explicitly in the Engulf number, it does affect both the liquid foam viscosity $\mu_D$ and the gas generation pressure $p_G$. According to (3.8), the liquid foam viscosity decreases exponentially as temperature increases. This trend is partially offset by the fact that the gas generation pressure *increases* with metal temperature. The net result, though, is that the Engulf number decreases by about half for every 50° increase in metal temperature.

Hill et al. [7] found that lowering foam density decreases porosity and folds. The Engulf number depends on the fourth power of the foam density (since $p_G$ is nearly linear in $\rho_F$), and so this result is also consistent with the idea that engulf mode is responsible for many fill-related anomalies.

Recently StyroChem began selling polystyrene beads (T175 and T185) containing an organic brominated additive that accelerates the rate of depolymerization upon heating [20]. Hess et al. [21] found that using brominated foam dramatically reduced the incidence of folds in actual castings. Since the brominated additive reduces the molecular weight of the polymer liquid, the effective viscosity $\mu_D$ is reduced accordingly. Foam pyrolysis data similar to that in Section 3 shows that brominated foam reduces the measured loads (and hence the effective viscosity) by almost an order of magnitude [10]. Therefore by substituting T175 foam for T170, the Engulf number can be substantially reduced. This explains why brominated beads have been so successful in reducing folds in lost foam casting of aluminum.

## 8. Discussion

The engulfing motion described in this paper is very likely responsible for many of the fill-related anomalies found in lost foam castings. It is caused by concave metal flow fronts that develop in response to the viscous resistance of the liquid foam in the decomposition layer. When the flow front becomes sufficiently concave, pieces of heat-softened foam inside the concave hollow of the flow front break off and become enveloped by liquid metal. The engulfed foam vaporizes very rapidly, creating large bubbles inside the molten metal just behind the flow front. If the gas in the bubble cannot escape through the coating before the metal solidifies, it leaves porosity in the casting. And even when the gas does escape, the oxides and carbon deposits that form on the surface of the bubble may not allow it to fuse properly after it collapses, creating a fold in the casting. Sometimes the bubble floats to the top of the cavity where it gets trapped under a thin skin of solidified metal. This creates a blister in the casting.

It is interesting to note that several researchers, even though they had only fragmentary, indirect evidence, have speculated that this kind of motion does in fact occur. Wang et al. [6] stated that, "At high metal velocities, the metal front tends to become unstable, sometimes even pulsing, making it easier to trap the foam." Hill et al. [7] spoke of "instabilities" that may "entrap liquid polymer." And Miller [3] talked about "unstable turbulence" at the flow front, causing the liquid metal to "engulf" or "entrap" pieces of foam. Although these authors felt that some kind of engulfing motion was taking place, they had only indirect evidence for it and did not speculate about its origin.

It is now clear that engulfing motion is caused by strongly concave flow fronts, which are brought on by several things, including faster filling speeds, lower metal temperatures, higher foam densities, and thicker casting sections. All these trends have been associated in the literature with increasing casting anomalies. The onset of engulf mode can be characterized by a single quantity, called the *Engulf number*. The Engulf number is more sensitive to some variables than it is to others. For example, the Engulf number depends on filling speed to the fourth power, which explains why experimenters have singled out this variable as especially important in controlling the occurrence of casting anomalies.

Engulf mode is intrinsically unsteady. After the liquid metal engulfs a piece of the foam pattern, it needs some time to "digest" the foam and reestablish a concave flow front. Eventually another piece of foam breaks free and the process starts all over again. This repetitive, somewhat random motion creates a pulsing effect that some experimenters have actually reported seeing. In essence, the metal "chews" its way through the pattern, engulfing small pieces of foam as it goes. Depending on the orientation of the pattern and flow direction relative to gravity, the bubbles that form may or may not obstruct further foam decomposition. For example, when a pattern is filled from the top-down, bubbles form behind and above the downward flowing metal and they do not interfere with the continuing engulfing motion at all. In bottom-up filling, on the other hand, buoyant forces cause the bubbles to rise with the flow front, where they must dissipate before the foam can decompose further. In this case, the foam decomposition mechanism may switch to gap mode [11].

Gravity can also affect when engulf mode begins. For example, in a vertical pattern filling from the top-down, a steady flow front never develops at all for Profile numbers greater than 65 (when $G = 1$), regardless of how small the Engulf number may be. So, while the Engulf number is a good guide for determining when engulf mode first begins, in some cases it is not the only factor that needs to be considered.

Finally, the theoretical development in this paper explains for the first time why brominated polystyrene foams create fewer casting anomalies than conventional foams. Since brominated foams degrade to liquids with lower molecular weights, the liquid foam in the decomposition layer has a much lower viscosity. This means that the flow front can be less concave (perhaps even convex) and still be able to force the decomposition products to the boundary. The Engulf number is reduced and engulf mode is put off to higher filling speeds.

The use of brominated polystyrene foam is only one way to reduce the Engulf number, however. Other ways include: lowering filling speeds by decreasing coating permeability, reducing the foam density, decreasing the pattern thickness, and increasing metal temperature. Not all these changes are possible in every instance, and some have a greater effect than others. But the theoretical development in this paper provides a framework for evaluating the effect of different process variables on the occurrence of engulf mode, together with the fill-related anomalies that it produces.

## Acknowledgement

The author would like to thank Dr. Taras Molibog, a former Ph.D. student at the University of Alabama at Birmingham, for sharing preliminary data from his foam pyrolysis experiments and for many useful and stimulating discussions on foam decomposition. Thanks are also due to Dr. Wayne Sun, also from UAB, who provided the X-ray images shown in Fig. 1. Finally the author is greatly indebted to Dr. Martin Barone, who graciously discussed this work throughout its development and offered many helpful suggestions.

## References

[1] J.R. Brown, The lost foam casting process, Met. Mater. 8 (1992) 550–555.
[2] Q. Zhao, T.W. Gustafson, M. Hoover, M.C. Flemings, Fold formation in the lost foam aluminum process. In: S.K. Das (Ed.), Aluminum 2003, TMS, Warrendale, 2003, pp. 121–132.
[3] B.A. Miller, Pattern Pyrolysis Defect Reduction in Lost Foam Castings, Masters Thesis, University of Alabama, Birmingham, Alabama, 1996.
[4] Q. Zhao, J.T. Burke, T.W. Gustafson, Foam removal mechanism in aluminum lost foam casting, AFS Trans. 110 (2002) 1399–1414.
[5] W.L. Sun, H.E. Littleton, C.E. Bates, Real-time X-ray investigations on lost foam mold filling, AFS Trans. 110 (2002) 1347–1356.
[6] C. Wang, C.W. Ramsay, D.R. Askeland, Processing variable significance on filling thin plates in the LFC process—the staggered, nested factorial experiment, AFS Trans. 105 (1997) 427–434.
[7] M. Hill, A.E. Vrieze, T.L. Moody, C.W. Ramsay, D.R. Askeland, Effect of metal velocity on defect formation in Al LFCs, AFS Trans. 106 (1998) 365–374.
[8] M.R. Barone, D.A. Caulk, A foam ablation model for lost foam casting of aluminum, Int. J. Heat Mass Transfer 48 (2005) 4132–4149.
[9] T.V. Molibog, H. Littleton, Degradation of expanded polystyrene patterns, AFS Trans. 110 (2002) 1483–1496.
[10] T.V. Molibog, H. Littleton, Experimental simulation of pattern degradation in lost foam, AFS Trans. 109 (2001) 1523–1554.
[11] D.A. Caulk, A foam melting model for lost foam casting of aluminum, Int. J. Heat Mass Transfer 49 (2006) 2124–2136.
[12] S. Katashima, S. Tashima, R.-S. Yang, Fluidity of Molten Silumin in the evaporative pattern casting process, AFS Trans. 97 (1989) 545–552.
[13] Z. Liu, J. Hu, W. Ding, Q. Wang, Y.G. Zhu, Y. Lu, W. Chen, Effect of processing parameters on mold filling in magnesium alloy EPC process, AFS Trans. 109 (2001) 1425–1438.
[14] M.H. Warner, B.A. Miller, H.E. Littleton, Pattern pyrolysis defect reduction in lost foam castings, AFS Trans. 106 (1998) 777–785.
[15] Y. Sun, H.L. Tsai, D.R. Askeland, Effects of silicon content, coating materials and gating design on casting defects in the aluminum lost foam casting process, AFS Trans. 104 (1996) 271–279.
[16] L. Wang, S. Shivkumar, D. Apelian, Effects of polymer degradation on the quality of lost foam castings, AFS Trans. 198 (1990) 923–933.
[17] M.W. Hill, M. Lawrence, C.W. Ramsay, D.R. Askeland, Influence of gating and other processing parameters on mold filling in the LFC process, AFS Trans. 105 (1997) 443–450.
[18] M.A. Tschopp, C.W. Ramsay, D.R. Askeland, Processing variable significance on metal flow and defect formation in thick section LFCs—full factorial experiment, AFS Trans. 108 (2000) 267–274.
[19] S. Bennett, T. Moody, A. Vrieze, M. Jackson, D.R. Askeland, C.W. Ramsay, Pyrolysis defects in aluminum lost foam casting, AFS Trans. 107 (1999) 795–803.
[20] F. Sonnenberg, Recent innovations with EPS lost foam beads, AFS Trans. 111 (2003) 1213–1229.
[21] D.R. Hess, D.R. Askeland, C.W. Ramsay, Influence of bead chemistry on metal velocity and defect formation in aluminum lost foam casting, AFS Trans. 111 (2003) 1425–1438.